Engineering Research Express

PAPER

Shape measurement of large thickness glass plates with a white-light scanning interferometer using a compensation glass and a fixed reference surface

To cite this article: Kaining Zhang *et al* 2021 *Eng. Res. Express* **3** 025044

IOP Publishing Eng. Res. Express 3 (2021) 025044 https://doi.org/10.1088/2631-8695/ac09d8

Engineering Research Express

CrossMark

RECEIVED
12 March 2021

REVISED
12 May 2021

ACCEPTED FOR PUBLICATION
9 June 2021

PUBLISHED
21 June 2021

PAPER

Shape measurement of large thickness glass plates with a white-light scanning interferometer using a compensation glass and a fixed reference surface

Kaining Zhang[1,2], Samuel Choi[2], Osami Sasaki[1,2], Songjie Luo[1], Takamasa Suzuki[2], Yongxin Liu[1] and Jixiong Pu[1]

[1] Fujian Provincial Key Laboratory of Light Propagation and Transformation, College of Information Science and Engineering, Huaqiao University, Xiamen, Fujian 361021, People's Republic of China
[2] Graduate School of Science and Technology, Niigata University, Niigata 950-2181, Japan

E-mail: Jixiong@hqu.edu.cn

Keywords: white-light scanning interferometer, thickness measurement, phase detection

Abstract

Conventional white-light scanning interferometers cannot measure exactly large thickness of glass plates because of a great dispersion effect. In this paper a compensation glass plate is used to reduce the dispersion effect. Moreover, a fixed reference surface is added behind the object and four-step measurements are performed. By this method a front surface profile and a thickness distribution of the object can be measured exactly without knowing the refractive index of the object, the thickness of the compensation glass, and dispersion effect containing in the interferometer. Due to the difficulty in scanning the reference surface at a constant speed over a long distance for a large thickness of the object, a piezoelectric transducer stage with a high positioning resolution are utilized together with an additional interferometer which measures the movement of this stage. Experimental results show that the error in thickness measurement is less than 60 nm and 170 nm for 1 mm and 5 mm-thickness glass plates, respectively.

1. Introduction

White-light scanning interferometers (WLSIs) have been used to measure a front surface profile and a thickness distribution of a transparent object [1–5]. The measurement of a thickness distribution involved with refractive index of an object is more difficult than the measurement of a front surface profile because a beam from the rear surface causes a large spread and distortion in the interference signal. This blurred interference signal makes it difficult to measure exactly the position of the rear surface of the object. For measuring a large thickness a compensation component is required to reduce the dispersion effect of an object. To the best of our knowledge, measurements of thickness more than 100 microns with an error less than 60 nm have not been reported except Ref. 4 in which a dual scanning white-light interferometer with two scanning reference surfaces was proposed and one point measurements of thickness of 1 mm were made. On the other hand, spectral resolved interferometers (SRIs) can measure so large thickness up to 3 mm with a high-resolution spectral analyzer and without a compensation component, as reported by many papers [6–11]. But SRIs limit the measurement region to one point or one line. Thus WLSIs play a significant role in the measurement of two-dimensional distributions.

In this paper a new WLSI having one scanning reference surface and a fixed reference surface is proposed to measure three-dimensional shape of glass plates with large thickness of 1 mm and 5 mm. The configuration of this WLSI is simpler than that proposed in [4]. A slope of a least square line in the spectral phase distribution of the interference signal is calculated. The following four-step measurements are performed: (1) A slope value produced by the front surface is measured in step 1. (2) By putting a compensation glass plate in front of the scanning reference surface, a slope value produced by the rear surface is measured in step 2. (3) By adding a fixed

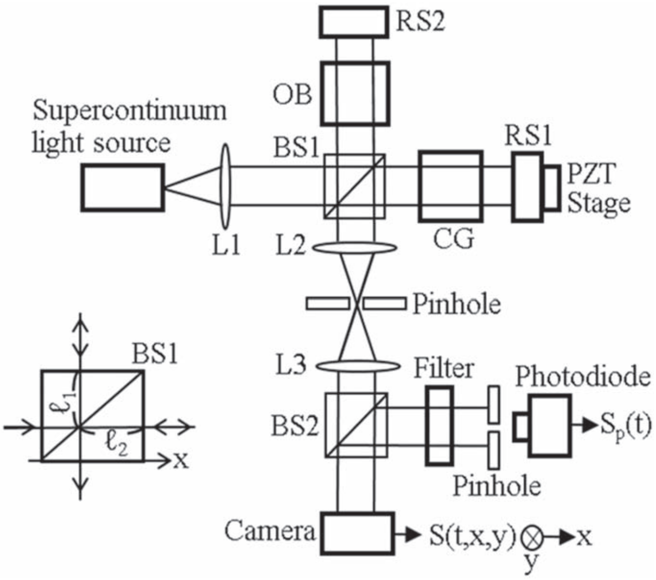

Figure 1. Schematic configuration of white-light scanning interferometer.

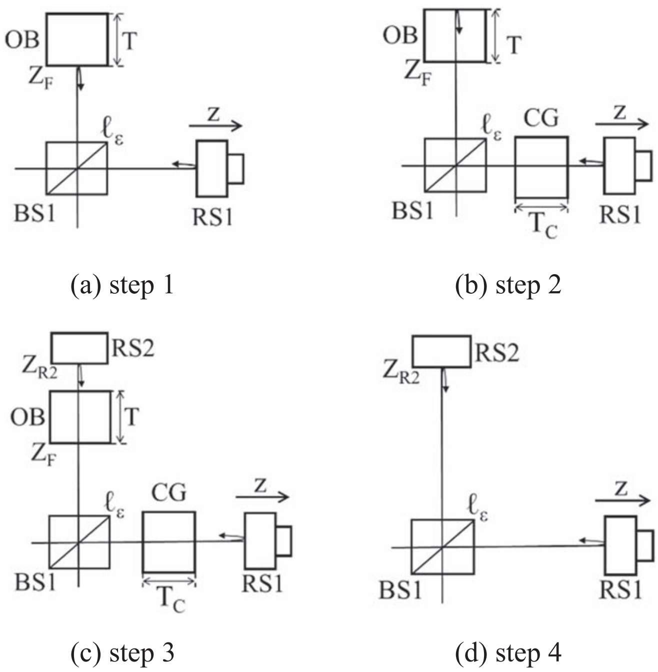

Figure 2. Four-step measurements and configurations in each step.

reference surface behind the object, a slope value generated from the interference between the fixed and scanning reference surfaces is measured in step 3. (4) Step 4 is the same as step 3 except that the object and the compensation glass plate do not exist. A thickness distribution is obtained from the four values of the slopes without knowing the refractive index of the object, the thickness of compensation glass, and dispersion effect containing in the interferometer. It is very important to scan accurately the reference surface for the object, but it is difficult to scan the reference surface at a constant speed over a long distance of a few millimeters. A piezoelectric transducer stage (PZTS) with a high positioning resolution is employed to reduce the scanning distance. Before detecting the interference signals, a displacement is given to the reference surface by the PZTS so that a short optical path difference (OPD) is produced in each step of the measurement. In order to measure the scanning positions of the reference surface, an additional interferometer is equipped in the WLSI [12]. By using the measured scanning positions the interference signal detected along time is converted to that along the accurate scanning positions.

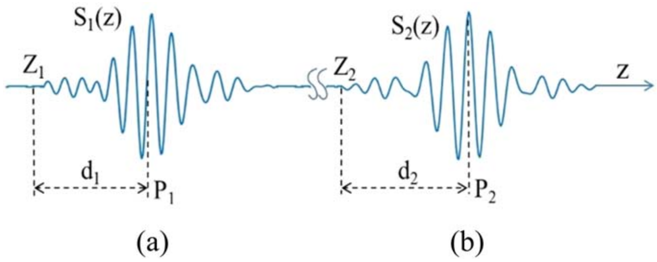

Figure 3. Interference signal in (a) step 1 and (b) step 2.

2. Principle

Figure 1 shows schematic configuration of a WLSI with a supercontinuum light source. There is a scanning axis in a reference arm which consists of a compensation glass (CG), a reference surface 1 (RS1), and a piezoelectric transducer (PZTS). The RS1 is moved by the PZTS, and a reference surface 2 (RS2) is fixed in an object arm. A beam collimated with a lens 1 (L1) is divided by a beam splitter 1 (BS1) for the object and reference arms. The two beams from the two arms are combined again by the BS1 and are divided by a beam splitter 2 (BS2). An interference signal of the WLSI is detected with a camera on which optical fields on the reflecting surfaces in the object and reference arms are formed with two lenses of L2 and L3. Another interference signal for measuring the movement of the RS1 is detected with a photodiode by passing the two beams through an optical band-path filter and a pinhole.

Shape measurement is made by four-step measurements as shown in figure 2. In step 1, the CG does not exist in the reference arm to measure position Z_F of the front surface of OB by scanning the position z of RS1. Since the BS1 has two sides of unequal length, the object and reference beams have different paths of l_1 and l_2 in the BS1, respectively, as shown in figure 1. Path difference of $l_\varepsilon = l_1 - l_2$ is a linear function along the x-axis [13]. Hence the OPD between the two beams coming from the object and reference arms contains $2n_B(\sigma)l_\varepsilon$, where $n_B(\sigma)$ is the refractive index of the BS1. Then the OPD is equal to $2[z + n_B(\sigma)l_\varepsilon - Z_F]$ in step 1, and the interference signal is expressed as

$$S_1(z) = \int \mathrm{I}(\sigma)\cos[4\pi(z + n_B(\sigma)l_\varepsilon - Z_F)\sigma]d\sigma, \tag{1}$$

where $I(\sigma)$ is the spectral intensity of light source and σ is wavenumber. Fourier transform of $S_1(z)$ in a region of positive wavenumber is given by

$$F_1(\sigma) = \mathrm{I}(\sigma)e^{j4\pi n_B(\sigma)l_\varepsilon\sigma}e^{-j4\pi Z_F\sigma}. \tag{2}$$

The linear component of the spectral phase distribution in equation (2) is equal to $4\pi[-Z_F\sigma + \text{linear}\{n_B(\sigma)l_\varepsilon\sigma\}]$, where linear$\{f(\sigma)\}$ means a linear component of the distribution $f(\sigma)$. The linear component of the spectral phase distribution is obtained with the least square method. The linear$\{n_B(\sigma)l_\varepsilon\sigma\}$ is expressed by $C_Bl_\varepsilon\sigma$, where the constant coefficient C_B depends on the distribution of $n_B(\sigma)$ [4]. Therefore, denoting the slope of the linear component of the spectral phase distribution in equation (2) by g_1, the measurement value P_1 in step 1 is given by

$$P_1 = -g_1/4\pi = Z_F - C_B l_\varepsilon. \tag{3}$$

The value P_1 is the position where the envelope peak of the interference signal $S_1(z)$ exists [13]. Figure 3(a) shows the signal $S_1(z)$ where the measurement value P_1 is indicated. Because $C_B\,l_\varepsilon$ expresses a flat plane inclined along the x-axis, the front surface profile Z_F is obtained by eliminating the inclination of the distribution P_1 along the x-axis. In step 2, the CG is put into the reference arm, and the refractive index of the OB and CG is $n(\sigma)$. The interference signal $S_2(z)$ is generated by the beams reflected from the rear surface of OB and the RS1, and the OPD in $S_2(z)$ is equal to $2[z + n_B(\sigma)l_\varepsilon + (n(\sigma) - 1)T_C - n(\sigma)T - Z_F]$, where T and T_C are the thickness of OB and CG, respectively. Figure 3(b) shows the signal $S_2(z)$ with the measurement value P_2. The linear component of the spectral phase distribution of $S_2(z)$ is equal to $4\pi[C_Bl_\varepsilon - C_S(T - T_C) - T_C - Z_F]\sigma$, where $C_ST\sigma$ is the linear component of $n(\sigma)T\sigma$. In the same way as in step 1, from the slope of the spectral phase, the measurement value P_2 is given by

$$P_2 = Z_F + T_C - C_B l_\varepsilon + C_S T_S, \tag{4}$$

where $T_S = T - T_C$. From equations (3) and (4), the following measurement value is obtained in step 1 and step 2:

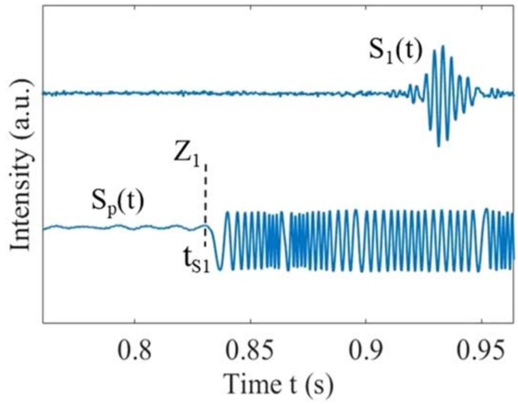

Figure 4. Detected signals $S(t)$ and $S_p(t)$.

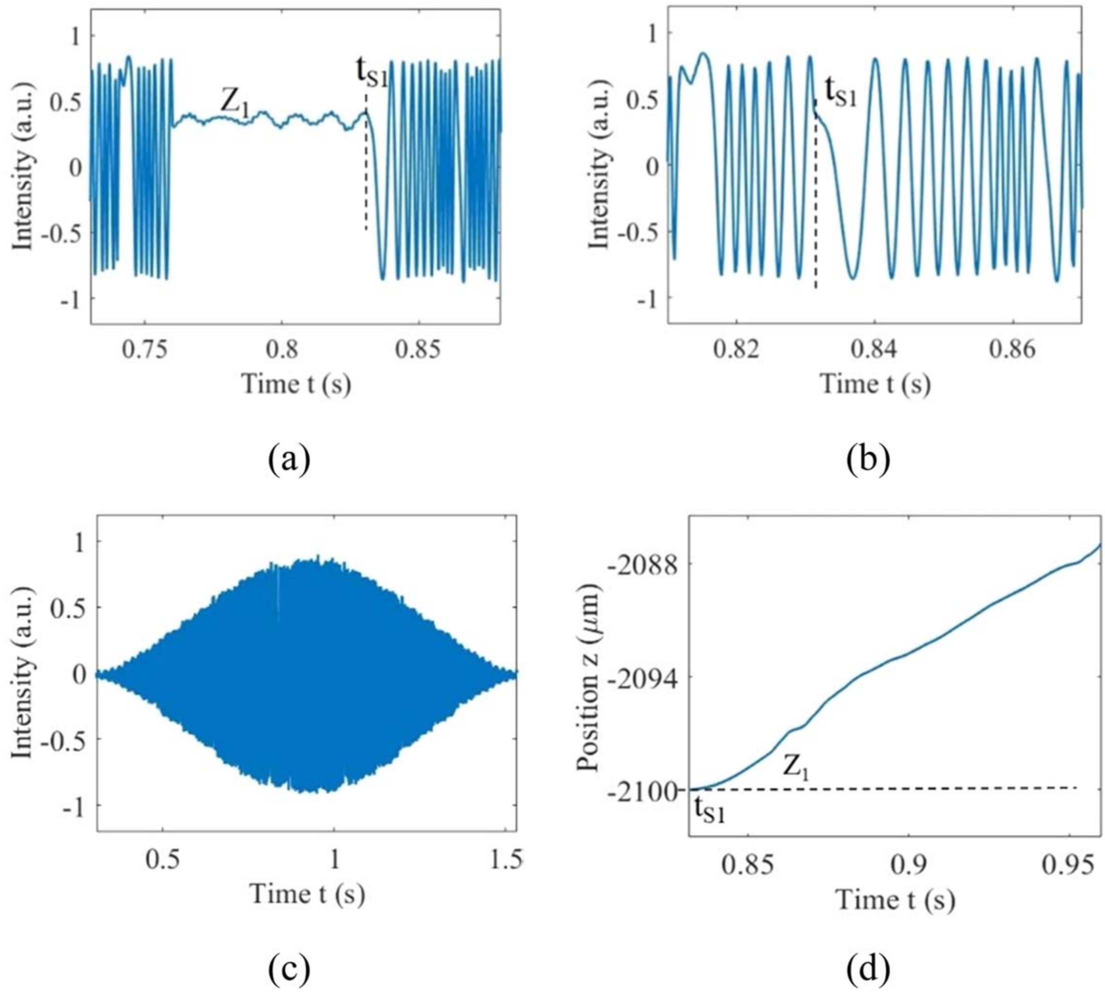

Figure 5. (a) Detected signal $S_p(t)$ around the stop position Z_1, (b) connected signal $S_p(t)$ by eliminating the stop region, (c) whole distribution of signal $S_p(t)$ after the connection, and (d) scanning positions of RS1 measured from $S_p(t)$.

$$D_1 = P_2 - P_1 = C_S T_S + T_C. \tag{5}$$

Figures 2(c) and (d) show step 3 and step 4 where the position of RS2 is denoted by Z_{R2}. In step 3, the interference signal is generated by the beams reflected from the RS1 and the RS2. The OPD in the interference signal is equal to $2[z + n_B(\sigma)l_\varepsilon + (n(\sigma) - 1)T_C - (n(\sigma) - 1)T - Z_{R2}]$. In the same way as in step 2 the measurement value P_3 are given by

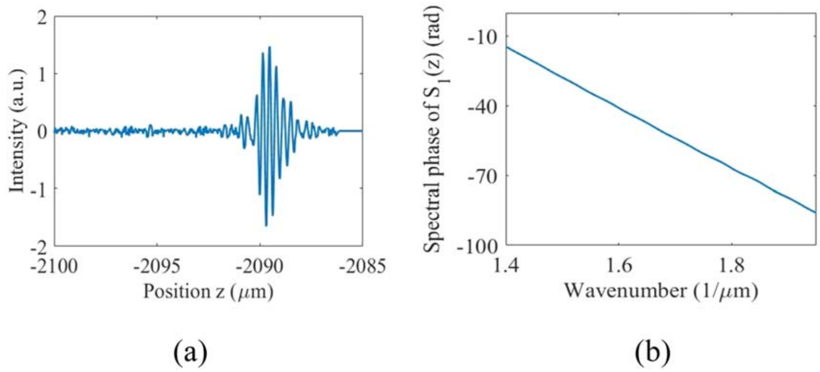

Figure 6. (a) Signal $S_1(z)$ converted from $S_1(t)$ by $S_p(t)$, and (b) spectral phase distribution of $S_1(z)$.

$$P_3 = Z_{R2} - T_S - C_B l_\varepsilon + C_S T_S. \tag{6}$$

In step 4, the OB and the CG are removed from the two arms, and the interference signal is generated by the beams reflected from the RS1 and the RS2. The OPD in the interference signal is equal to $2[z + n_B(\sigma)l_\varepsilon - Z_{R2}]$, and the measurement value P_4 are given by

$$P_4 = Z_{R2} - C_B l_\varepsilon. \tag{7}$$

From equations (6) and (7), the following measurement value is obtained in step 3 and step 4,

$$D_2 = P_3 - P_4 = (C_S - 1)T_S. \tag{8}$$

Finally from equations (5) and (8), the thickness T of OB is obtained as

$$D_1 - D_2 = T_C + T_S = T. \tag{9}$$

It should be denoted that the thickness T can be obtained from the four measurement values $P_i(i = 1-4)$ without using the coefficient C_S or the refractive index of the OB.

3. Experimental results

The WLSI was constructed as shown in figure 1, and shape measurements of glass plates were carried out. The RS1 and RS2 were glass plates with a wedged angle so that they were regarded as one reflecting surface. The RS1 was moved with a PZTS whose positioning resolution was 0.5 nm and average velocity was about 100 μm s^{-1}. The OB and the CG were glass plates of BK7, and their nominal values of thickness were the same ones. Interference signal $S(t,x,y)$ was detected by a high speed camera with one pixel size of 20 $\times$ 20 μm. The interval of measurement points was 200 μm by selecting one point every ten pixels along both x and y direction. The measuring point was denoted by N_x and N_y, where N_x was from 1 to 48 and N_y was from 1 to 36. At the same time, the interference signal $S_p(t)$ was detected by the photodiode [12], as shown in figure 1. The spectral range of the supercontinuum light was about 500–800 nm. The central wavelength $1/\sigma_f$ and bandwidth of the filter were 633 nm and 3 nm respectively. The signal $S_p(t)$ was transferred to a computer with an A/D converter. The frame rate of the camera and the sampling frequency of the photodiode were specified by a same signal of 5KHz. A start pulse for the camera and the photodiode was generated by a PZTS controller.

It is explained how to get an interference signal $S_1(z)$ of WLSI by showing the interference signal $S_1(t)$ on one measurement point of $N_x = 24$ and $N_y = 18$ and the interference signal $S_p(t)$ detected in step 1. These signals are shown in figure 4, where the detection of the signals started at $t = 0$ s. It is needed that time t is converted to scanning position z. The PZTS stops at a specified position of $z = Z_1$ with repeatability of about 10 nm, and the exact value of Z_1 can be obtained from the PZTS controller. Since the PZTS controller cannot continuously output the position z while the PZTS is moving, the signal $S_p(t)$ is used to measure the movement of the PZTS. A short movement less than 70 μm could be measured with the signal $S_p(t)$ because the coherence length of the signal $S_p(t)$ was about 70 μm. The signal $S_p(t)$ detected between $t = 0.73$ s and $t = 0.88$ s is shown in figure 5(a). The PZTS stopped at $t = 0.76$ s at position $Z_1 = -2100.000$ μm, and it moved again at $t_{S1} = 0.83$ s. The phase distribution of $S_p(t)$ is extracted through Fourier transform. But a continuous $S_p(t)$ having zero values on the both sides is required to obtain an exact phase distribution. Thus the signal $S_p(t)$ detected before $t = 0.76$ s was used and it was connected to the $S_p(t)$ starting at t_{S1} by eliminating the part of the almost constant signal. The connected signal $S_p(t)$ is shown in figure 5(b). And the whole signal of $S_p(t)$ after this connection is shown in figure 5(c). A wrapped phase distribution of the $S_p(t)$ was calculated by performing inverse Fourier transform on the distribution in the region of positive wavenumbers of Fourier transform of the signal $S_p(t)$. And the scanning

Table 1. Values measured with a CG of company A in Case 1 to 3 and with a CG of company B in Case 4. Thickness of the OB was 1 mm.

(μm)	Case1	Case2	Case3	Case 4
P_1	−2089.639	−2052.774	−2062.073	−2009.544
P_2	−1060.451	−1023.599	−1032.859	−992.315
D_1	1029.188	1029.175	1029.214	1017.229
P_3	5009.067	5009.084	5009.083	5007.054
P_4	4997.356	4997.328	4997.327	5007.245
D_2	11.711	11.756	11.755	−0.191
T	1017.476	1017.419	1017.459	1017.420

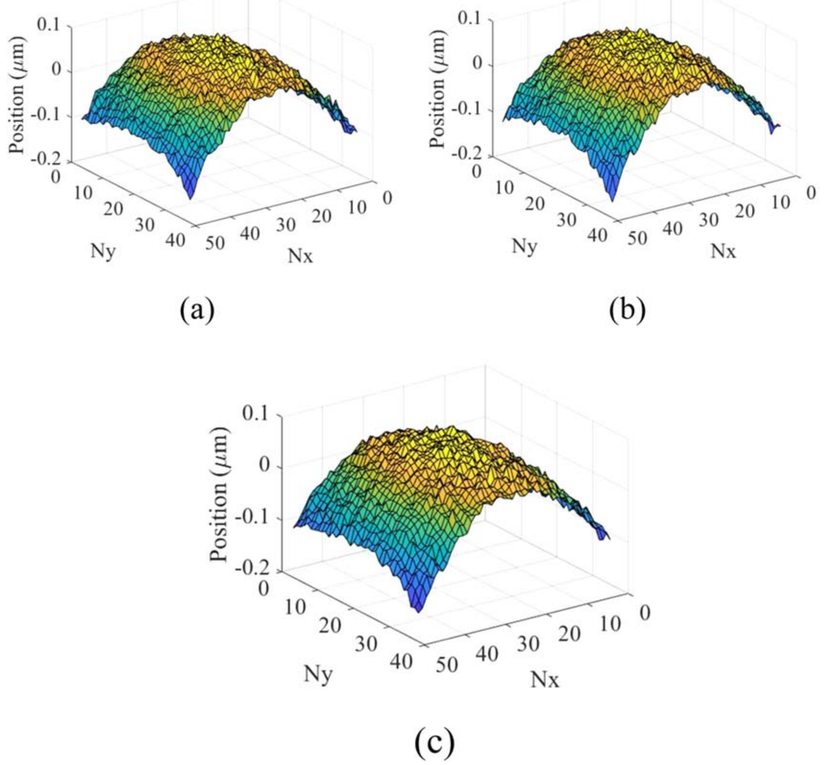

Figure 7. Front surface profiles of 1-mm thickness OB measured in (a) Case 1, (b) Case 2, and (c) Case 3.

position of the RS1 was obtained by dividing the unwrapped phase by $4\pi\sigma_f$, where $\sigma_f = 1/633\ \text{nm}^{-1}$. Figure 5(d) shows the measured result which indicates the non-constant speed of the RS1. The signal $S_1(t)$ with a sampling interval of 0.2 ms was converted to a signal $S_1(z)$ by using the relation shown in figure 5(d). After that, a signal $S_1(z)$ with a constant sampling interval of 20 nm was calculated with spline interpolation as shown in figure 6(a), where the first sampling point was at Z_1. A wrapped phase distribution of $F_1(\sigma)$ was calculated through performing Fourier transform on the $S_1(z)$. In the $S_1(z)$ zero values were added in the region outside $z = -2086.22\ \mu$m as shown in figure 6(a), so that the sampling interval in the wrapped phase distribution became to be small. Figure 6(b) shows the unwrapped phase distribution of $F_1(\sigma)$ or spectral phase distribution of $S_1(z)$, and its slope was -130.202 rad μm^{-1} which arose from the distance $d_1 = 130.202/4\pi = 10.361\ \mu$m between the signal position and the first sampling point of $Z_1 = -2100.000\ \mu$m. Therefore, the measurement value P_1 was equal to $Z_1 + d_1 = -2089.639\ \mu$m, as shown in figure 3. In step 2, after putting the CG into the reference arm, PZTS was moved to the specified stop position $Z_2 = -1070.000\ \mu$m. The PZTS was moved again from the position Z_2 to detect the interference signals $S_2(t)$ and $S_p(t)$. By doing the same signal processing as in step 1, the measurement value $P_2 = -1060.451\ \mu$m was obtained. In step 3 and 4, the signals $S_3(t)$ and $S_4(t)$ generated by the beams reflected from RS1 and RS2 were detected. In step 3, PZTS was moved to another specified stop position $Z_3 = 4997.000\ \mu$m to detect the interference signals $S_3(t)$ and $S_p(t)$. The measurement value $P_3 = 5009.067\ \mu$m was obtained. In step 4, the OB and the CG were removed from the interferometer and the PZTS was moved to the specified stop position $Z_4 = 4987.000\ \mu$m. The measurement value $P_4 = 4997.356$

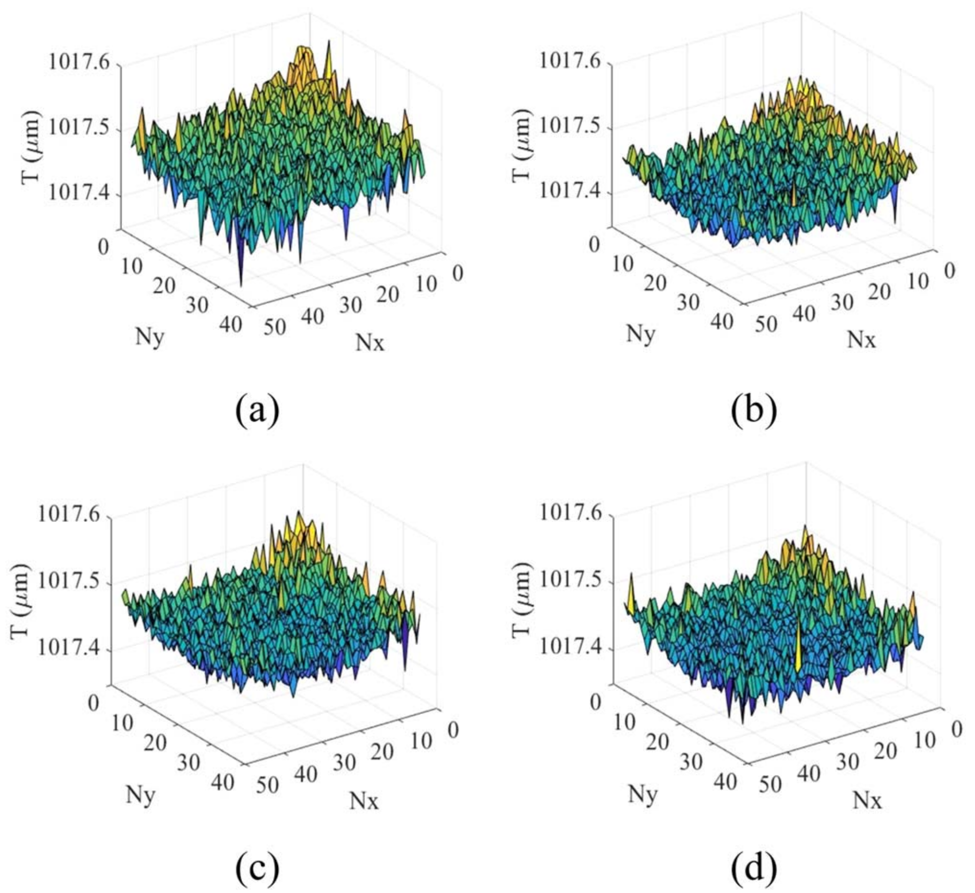

Figure 8. Thickness distributions of 1 mm-thickness OB measured with a CG of company A in (a) Case 1, (b) Case 2, and (c) Case 3. And (d) thickness distribution of the OB measured with a CG of company B.

Table 2. RMS difference R$\{Z_F\}$ between front surface profiles measured in two different cases. RMS difference R$\{T\}$ between thickness distributions. Thickness of the OB was 1 mm.

RMS difference (μm)	(a) and (b)	(b) and (c)	(c) and (a)	(c) and (d)
R$\{Z_F\}$	0.008	0.005	0.006	
R$\{T\}$	0.038	0.022	0.023	0.022

μm was obtained. From these detected values the thickness was measured as $T = 1017.476$ μm through the values of $D_1 = P_2 - P_1$ and $D_2 = P_3 - P_4$ in Case 1, as shown in table 1.

Three-dimensional shape measurement was repeated three times as Case 1, 2, and 3. A front surface profile Z_F of an OB was obtained by eliminating an inclination and a bias from the distribution $P_{1.}$ The front surface profiles measured in Case 1, 2, and 3 are shown in figures 7(a)–(c), respectively. The measured thickness distributions in Case 1, 2, and 3 are shown in figures 8(a)–(c), respectively. The nominal value of thicknesses of the OB and the CG produced by company A was 1 mm. The three front surface profiles were almost the same without large fluctuations, but the three thickness distributions have large fluctuations especially in the region near $N_x = 0$ and $N_y = 0$ where the beam intensity was weak. Figure 8(d) shows the thickness distributions measured with a different CG produced by company B. This distribution was almost the same as those measured with the CG produced by company A. In order to examine the experimental situations in details, values measured at the point of $N_x = 24$ and $N_y = 18$ in Case 1 to Case 3 are shown in table 1. Values P_1 were very different in the different cases because the position of OB changed in each case due to the removing of OB in step 4. But the difference of values D_1 in the different cases was less than 40 nm. This difference was caused by positioning error in Z_2 of the PZTS in the travel distance of about 1 mm and position change of the OB due to the inserting of the CG. Also the difference of values D_2 less than 45 nm was caused by positioning error in Z_4 of the PZTS in the travel distance of about 0.6 mm and position changes of the RS1 and RS2 due to the removing of the OB and the CG. Ultimately the difference of thickness T was less than 57 nm at one measurement point. In

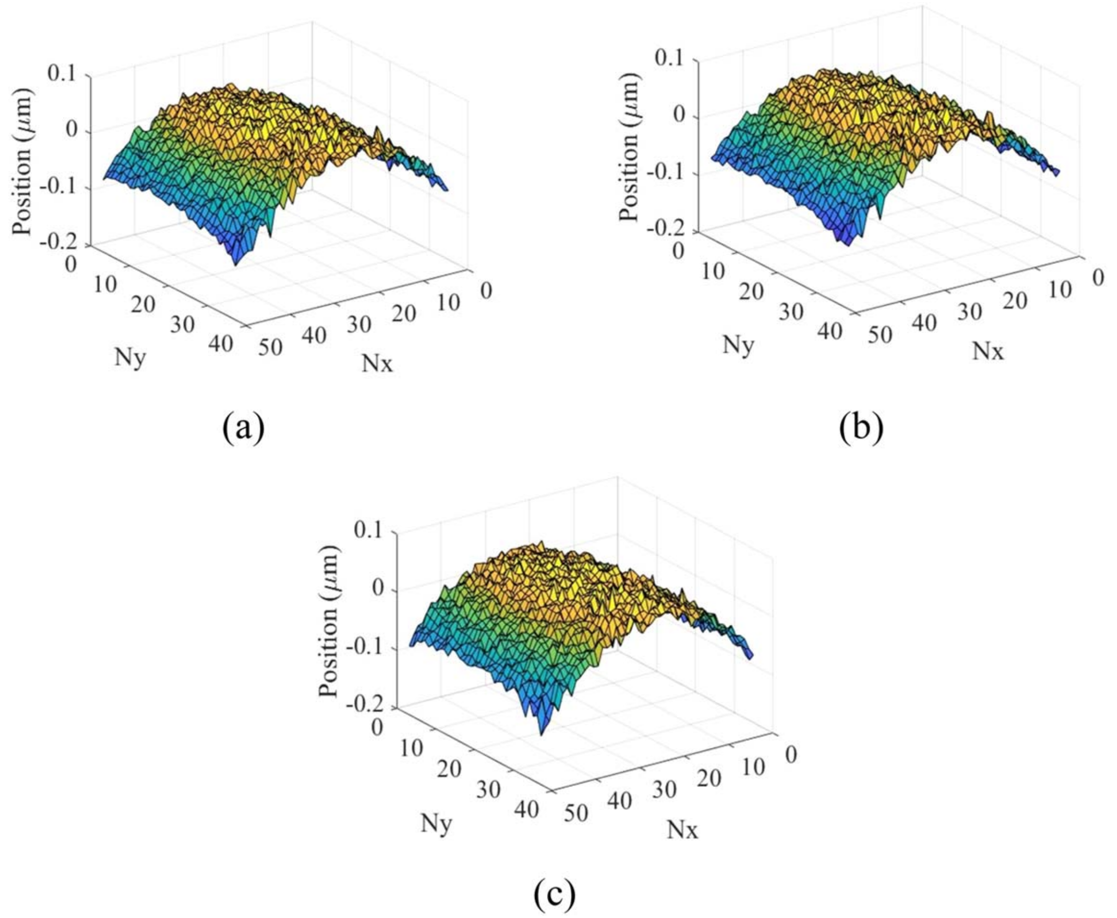

Figure 9. Front surface profiles of 5-mm thickness OB measured in (a) Case 1, (b) Case 2, and (c) Case 3.

Table 3. Values measured in three different cases. Thickness of the OB was 5 mm.

(μm)	Case1	Case2	Case3
P_1	−6570.342	−6567.912	−6603.740
P_2	−1173.584	−1171.062	−1206.890
D_1	5396.758	5396.850	5396.850
P_3	5085.840	5086.013	5086.667
P_4	4965.853	4966.044	4966.754
D_2	119.988	119.970	119.913
T	5276.770	5276.880	5276.937

Table 4. RMS difference R{Z_F} between front surface profiles measured in two different cases. RMS difference R{T} between thickness distributions. Thickness of the OB was 5 mm.

RMS difference (μm)	(a) and (b)	(b) and (c)	(c) and (a)
R{Z_F}	0.004	0.008	0.006
R{T}	0.089	0.068	0.158

table 1, Case 4 shows values measured with the CG of company B. The value of D_2 is related to the thickness of the CG with equation (8). Since the value of C_S-1 is about 0.5 [4], T_S is nearly equal to $2D_2$. Although the values of T_S were about 23 μm in Case 1 to 3 and -0.4 μm in Case 4, the values of T of the OB were almost the same value. These results indicate that it is acceptable that the thickness of CG is different from that of OB by a few tens of microns.

In order to estimate the repeatability in the two-dimensional distribution of the front surface profile and the thickness, RMS (root-mean-square) difference R{Z_F} and R{T} in the measured values of Z_F and T,

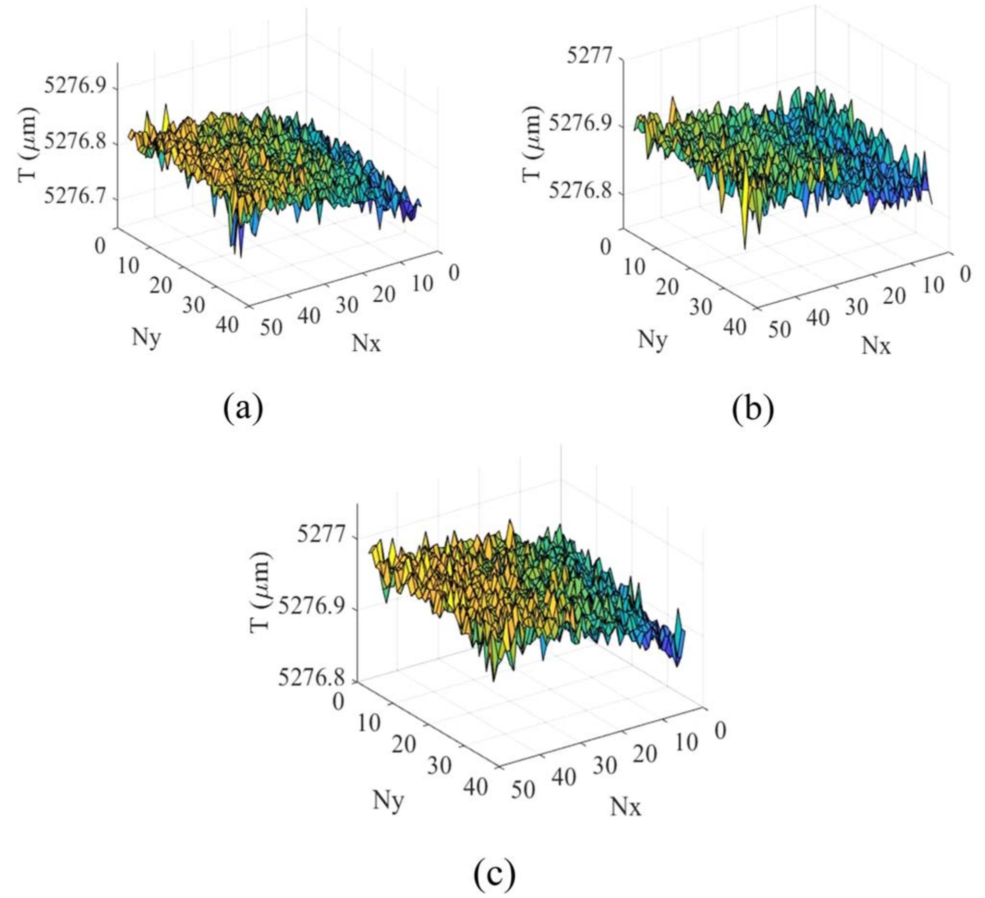

Figure 10. Thickness distributions of 5 mm-thickness OB measured in (a) Case 1, (b) Case 2, and (c) Case 3.

respectively, between two different cases are shown in table 2. The notations of (a)–(d) correspond to figures 7(a)–(c) in R$\{Z_F\}$ and figures 8(a)–(d) in R$\{T\}$, respectively. From the results in table 2 the repeatability values in front surface profile and thickness distribution were 6 nm and 26 nm, respectively.

The OB of 1 mm-thickness was changed to an OB of 5 mm-thickness in nominal value, and the same measurements were carried out. The front surface profiles measured in Case 1, 2, and 3 are shown in figures 9(a)–(c), respectively. The thickness distributions measured in Case 1, 2, and 3 are shown in figures 10(a)–(c), respectively. Table 3 shows values measured at the point of $N_x = 24$ and $N_y = 18$. The difference of values D_1 increased to less than about 100 nm. This increase was caused by the large travel distance of about 5 mm proportional to the thickness of the OB. The difference of values D_2 was less than 75 nm. Ultimately the difference of thickness T was less than 170 nm at one measurement point. RMS differences in the measured values of Z_F and T between different two cases are shown in table 4. From the results in table 4 the repeatability values in front surface profile and thickness distribution were 6 nm and 105 nm, respectively.

The repeatability of thickness distribution increased from 26 nm to 105 nm by the increases of thickness from 1 mm to 5 mm. A source of the measurement error or the repeatability of about 30 nm and 100 nm was the positioning error of the PZTS. Another error source was position change of the OB, the RS1, and the RS2 caused by the movements of the CG and the OB. From the experimental results shown in table 1 and table 2, it is estimated that the movements of the CG and the OB cause an error less than about 50 nm in D_1 and D_2. Also it is estimated that the positioning repeatability of the PZTS causes an error of about 10 nm in D_1 and D_2 per 1 mm travel distance of the PZTS.

4. Conclusion

The new WLSI was constructed by using a compensation glass plate, a fixed reference surface, the PZTS, and the additional interferometer. The front surface profiles and the thickness distributions of glass plates with 1 mm and 5 mm-thickness could be measured through the four-step measurements without using a value of the refractive index, the thickness of the compensation glass, and the dispersion effect of the BS. The error in the thickness measurement was less than 60 nm and 170 nm for 1 mm and 5 mm-thickness glass plates, respectively, at a center position of the measurement region. The measurement repeatability over the measurement region was about 6 nm in the front surface profile for both thickness glass plates, and it was about 30 nm and 100 nm in the thickness distribution for 1 mm and 5 mm-thickness glass plates, respectively. Since the maximum measurable thickness depends on the travel distance of the PZTS in principle, the measurements of thickness larger than 5 mm will be carried out in the near future.

Acknowledgments

The authors would like to thank the supports by National Natural Science Foundation of China (NSFC) (No. 11674111, No. 61575070, No. 11750110426, No. 62005086).

Data availability statement

All data that support the findings of this study are included within the article (and any supplementary files).

Conflict of interest

The authors declare no conflicts of interest.

ORCID iDs

Jixiong Pu https://orcid.org/0000-0001-8781-6683

References

[1] De Groot P and De Lega X C 2008 Scanning interferometry for thin film thickness and surface measurements *U.S. patent.* 7,324,210 B2
[2] Ma L, Guo T, Yuan F, Zhao J, Fu X and Hu X 2009 Thick film geometric parameters measurement by white light interferometry *Proc. SPIE* **7507** 75070GI 1
[3] Park H M and Joo K 2017 High-speed combined NIR low-coherence interferometry for wafer metrology *Appl. Opt.* **56** 8592
[4] Zhang K, Sasaki O, Luo S, Suzuki T, Liu Y and Pu J 2020 A dual-scanning white-light interferometer for exact thickness measurement of a large-thickness glass plate *Meas. Sci. Technol.* **31** 045009
[5] Luo S, Sasaki O, Choi S, Suzuki T, Chen Z and Pu J 2021 Shape measurement of a thin glass plate through analyzing dispersion effects in a white-light scanning interferometer *Opt. Lasers Eng.* **139** 106505
[6] Joo K and Kim S 2006 Absolute distance measurement by dispersive interferometry using a femtosecond pulse laser *Opt. Express* **14** 5954
[7] Jin J, Kim J W, Kang C, Kim J and Eom T 2010 Thickness and refractive index measurement of a silicon wafer based on an optical comb *Opt. Express* **18** 18339
[8] Na J, Choi H Y, Choi E S, Lee C and Lee B H 2009 Self-referenced spectral interferometry for simultaneous measurements of thickness and refractive index *Appl. Opt.* **48** 2461
[9] Park S J, Park K S, Kim Y H and Lee B H 2011 Simultaneous measurements of refractive index and thickness by spectral-domain low coherence interferometry having dual sample probes *IEEE. Photonics. Tech. L.* **23** 1076
[10] Maeng S, Park J, Byungsung Oh and Jin J 2012 Uncertainty improvement of geometrical thickness and refractive index measurement of a silicon wafer using a femtosecond pulse laser *Opt. Express* **20** 12184
[11] Park J, Mori H, Jang Y S and Jin J 2020 Precise thickness profile measurement insensitive to spatial and temporal temperature gradients on a large glass substrate *Appl. Opt.* **59** 5881
[12] Luo S, Suzuki T, Sasaki O, Choi S, Chen Z and Pu J 2009 Signal correction by detection of scanning position in a white-light interferometer for exact surface profile measurement *Appl. Opt.* **58** 3548
[13] Luo S, Sasaki O, Chen Z, Choi S and Pu J 2018 Exact surface profile measurement without subtracting dispersion phase through fourier transform in a white-light scanning interferometer *Appl. Opt.* **57** 894